Separation and Purification Technology 137 (2014) 74–81

Contents lists available at ScienceDirect

Separation and Purification Technology

journal homepage: www.elsevier.com/locate/seppur

Effect of various zinc oxide nanoparticles in membrane photocatalytic reactor for Congo red dye treatment

Nur Hanis Hayati Hairom [a,c], Abdul Wahab Mohammad [b,*], Abdul Amir Hassan Kadhum [b]

[a] Department of Chemical Engineering Technology, Faculty of Engineering Technology, Universiti Tun Hussein Onn Malaysia, 86400 Parit Raja, Batu Pahat, Johor, Malaysia
[b] Centre for Sustainable Process Technology (CESPRO), Faculty of Engineering and Built Environment, Universiti Kebangsaan Malaysia, 43600 UKM Bangi, Selangor, Malaysia
[c] Department of Chemical and Process Engineering, Faculty of Engineering and Built Environment, Universiti Kebangsaan Malaysia, 43600 UKM Bangi, Selangor, Malaysia

ARTICLE INFO

Article history:
Received 6 August 2014
Received in revised form 8 September 2014
Accepted 10 September 2014
Available online 30 September 2014

Keywords:
Membrane photocatalytic reactor
Zinc oxide
Nanoparticles
Congo red
Fouling

ABSTRACT

The utilisation of titanium dioxide (TiO_2) in a coupling system membrane photocatalytic reactor (MPR) has been widely investigated. However, there have been very few studies regarding the zinc oxide (ZnO) photocatalyst in MPR, although it has been shown to provide better efficiency than TiO_2 in certain cases, mainly for dye photodegradation. In this study, the influence of ZnO nanoparticles in MPR has been investigated for Congo red (CR) dye treatment. Four types of ZnO were synthesised via the precipitation of oxalic acid and zinc acetate solutions. The X-ray diffractometry (XRD) and transmission electron microscopy (TEM) results showed that precipitation is a valuable method for producing the smallest particle size (7–30 nm) of ZnO without any agglomerations, especially under stirring conditions in the presence of PVP (ZnO-PVP-St). As expected, the ZnO-PVP-St presented the great potential in MPR in terms of the highest photodegradation efficiency and lesser membrane flux decline, which was supported by the FESEM results. From the EDX analysis, it was confirmed that the small amount of ZnO-PVP-St did not pass through the membrane pores to the final stream. It was believed that the other remaining ZnO was reused in the photocatalytic reactor, for the continuous process of MPR. Due to the effective surface area of ZnO-PVP-St and adsorption of UV light, the optimum photocatalyst loading for the system was 0.3 g L^{-1} under 20 mg L^{-1} dye concentration and pH 7 of the initial CR dye solution.

1. Introduction

Coupling membrane technology with photocatalytic degradation system, the membrane photocatalytic reactor (MPR) is an advanced alternative to the conventional treatment method. In the coupling system, photocatalytic degradation acted as the pretreatment process where it can reduce the membrane fouling and flux decline. Membrane filtration replaced the sedimentation process in conventional methods, and acted as a barrier to the photocatalyst and some molecules/ions from being transported in the final stream. MPR consumption can save energy and reduce the installation size since it does not require additional operations such as coagulation, flocculation and sedimentation [1]. In addition, other advantages of this system include simple configuration, better process control, good efficiency, continuous process (photocatalyst and the product can be separated at the same time) and the potential reuse of the photocatalyst [2]. Generally, the catalysts used in coagulation, flocculation and sedimentation cannot be used again.

To date, MPR has attracted much attention due to their advantages. However, almost all of the previous studies were focused on the utilisation of titanium dioxide (TiO_2) as the photocatalyst, due to its effectiveness [3–5]. Recently, Hairom et al. [6] reported the utilisation of zinc oxide (ZnO) nanoparticles in MPR for industrial dye wastewater treatment using UF and NF membranes [6]. They found that the chemical properties of the effluent and nanofiltration (NF) membrane performance were improved in the presence of their ZnO via precipitation methods. In addition, they concluded that ZnO nanoparticles have great potential in MPR for dye treatment. ZnO is already known to be an effective photocatalyst due to its strong excitation binding energy and advantages [7,8]. However, it is very rarely used in MPR. In 2006, Kanade et al. [9] claimed that the characteristics of ZnO powder are dependent on its size and methods of preparation. The statement was supported by a recent report [10] which confirmed that the photocatalytic activity of ZnO nanoparticles is very sensitive to precursors and synthesis process conditions. Therefore, it can be concluded that the preparation of ZnO may influence the photocatalysis

* Corresponding author.
E-mail addresses: nurhanishayati@gmail.com (N.H.H. Hairom), wahabm@eng.ukm.my (A.W. Mohammad), amir@eng.ukm.my (A.A.H. Kadhum).

http://dx.doi.org/10.1016/j.seppur.2014.09.027
1383-5866/

performance in MPR and subsequently affect the characteristics of the membrane during the filtration process [6]. In order to investigate the impact of the issue in MPR, this study intends to investigate the effect of various types of ZnO via precipitation methods in MPR.

Precipitation process is the production of a solid in solution through a chemical reaction between the reactants. The solid formed in a liquid solution is called a precipitate. Typically, the precipitate will remain in suspension as the force of gravity is not sufficient to bring the solid particles down to the bottom. Therefore, the solid can be obtained through processes such as filtration, centrifugation, etc. The advantages of these processes are the fact that they are simpler routes, inexpensive, energy saving (room temperature) and produce good yields with uniform shapes and sizes. Previously, three different conditions of precipitation method were studied by Behnajady et al. for producing ZnO nanoparticles [10]. They observed that the reaction between zinc acetate ($Zn(CH_3COO)_2{\cdot}2H_2O$) and oxalic acid ($H_2C_2O_4{\cdot}2H_2O$) in ethanol solvent under ultrasonic radiation obtained the best performance for ZnO in the photocatalysis process. Kanade et al. reported the effect of solvents (water, methanol and ethylene glycol) on the precipitation synthesis of nano-sized ZnO using zinc acetate and oxalic acid under vigorous stirring at room temperature [9]. They found that the same percentage, 90% of ZnO was obtained from zinc oxalate for all of the different solvents. Hence, this study attempts to synthesise ZnO nanoparticles through the reaction between zinc acetate and oxalic acid in water solvent under stirring conditions and ultrasonic radiation at room temperature.

One of the serious problems faced in the synthesis of nanoparticles is 'agglomeration'. Agglomeration is the process resulting from the Ostwald ripening and Vander Waals interactions between nanoparticles when the particle growth is not controlled [11]. Agglomeration can be prevented by stabilising them electrostatically in suitable phases to achieve the selected size [12]. A current trend in view of reducing the agglomeration is capping the nanoparticles using polyvinyl pyrrolidone (PVP) as a stabilising agent [13,14]. PVP is a water-soluble polymer, consisting of an N-vinyl pyrrolidone monomer that can form a bond with the Zn ions on the growing particles, leading to prevention of the aggregation of nanoparticles. Furthermore, it has been reported that PVP not only controls the shape and particle size, but also improves the luminescence properties of several nanoparticles [15,16]. Therefore, the effect of PVP in the precipitation of ZnO was also studied in this report. The main objective of ZnO production is to obtain much smaller ZnO nanoparticles without any agglomeration via a simple method. This is essential in order to acquire a better performance of photocatalysts in MPR.

Most of the MPRs for dye purification described in the literature have used pressure-driven membrane processes including microfiltration (MF) [17,18], ultrafiltration (UF) [19,20] and nanofiltration (NF) [21,22]. However, severe membrane fouling is observed in the case of MF and UF membranes when a suspension photocatalyst was applied in MPR [23]. In addition, the lower quality of permeate was obtained since small particles/molecules/ions can pass easily through the membranes during the both microfiltration and ultrafiltration [6,23]. Thus, an NF membrane was used in this work in order to ensure the effectiveness of the MPR system and the quality of permeate.

Congo red (CR) dye was used in this study as the model of synthetic dye. This is because CR was frequently used in the dyeing process for many industries such as textiles, leather, food, paper, printing, pharmaceutical, cosmetics, etc. However, the waste water produced from these industries involving CR has contributed to serious environmental issues due to its natural aesthetic, where the colours can be seen even at low concentrations [24]. The reactive azo CR dye, which is also difficult to biodegrade, was not affected by the conventional treatment. Therefore, pollution caused by industries involving CR may become a huge problem in the future without proper pollution control.

2. Materials and methods

2.1. Synthesis and characterisation of ZnO nanoparticles via the precipitation method

Here, 0.15 M solution of oxalic acid dehydrate (purchased from R&M Marketing, Essex, U.K) was added slowly to 0.1 M solution of zinc acetate dehydrate (purchased from R&M Marketing, Essex, U.K) (molar ratio of oxalic acid to zinc acetate is 1.5) at room temperature (25 °C) under four different conditions:

(i) vigorous stirring without PVP (ZnO-St),
(ii) ultrasonic radiations without PVP (ZnO-Us),
(iii) vigorous stirring in the presence of PVP (ZnO-PVP-St) and
(iv) ultrasonic radiations in the presence of PVP (ZnO-PVP-Us).

For the preparation of ZnO-PVP-St and ZnO-PVP-Us, 0.015 g/L PVP (purchased from R&M Marketing, Essex, U.K.) was added to the mixture after 5 min of reaction. The precipitate obtained was filtered and then calcined in the furnace (Nabertherm model, Germany) under 550 °C (3 h) in order to remove impurities. Commercial ZnO purchased from Sigma Aldrich, USA was used for comparison purposes. Physical and chemical properties of the nanoparticles were characterised with X-ray diffractometry (XRD) (Bruker AXS GmbH model) and transmission electron microscopy (TEM) (CM12 Philips model).

2.2. Membrane and its characterisation

Polypiperazine amide NF membrane (GE Osmonics®, Trisep® TS40, USA) was used in this study. The characteristics of the membranes are tabulated in Table 1. The new membrane sample was immersed in reverse osmosis (RO) water over-night before it was used in the reactor. Morphology of the membrane surface and cross-sections were observed with field emission scanning electron microscopy (FESEM; Gemini, SUPRA 55VP-ZEISS) equipped with an energy dispersive X-ray (EDX) analysis system. For the cross-sectional analysis, small pieces of the membranes were soaked in an appropriate amount of liquid nitrogen for 4–5 h. The samples were fractured and dried in an oven under 60 °C. The dried samples were coated with gold to generate the electrical conductivity. Afterwards, observation of the prepared samples was carried out with the microscope at 3 and 10 kV. Analysis of the element intensity on the membrane surface was conducted with the EDX system.

2.3. Congo red dye

Congo red (CR) dye powder (molecular weight: 696.66 g/mol) was obtained from R&M Chemicals, United Kingdom (U.K.) and

Table 1
Characteristics of the NF membrane.

Membrane	Characteristic
MWCO[a]	200 Da
Na_2SO_4 rejection[b]	99%
NaCl rejection[b]	10–40%
pH tolerance[a]	2–12
Standard operation pressure[a]	2–14 bar
Hydrophobicity[b]	Hydrophilic
Contact angle (°)[b]	39.0 ± 1.5

[a] Information obtained from manufacturer.
[b] Value obtained from experimental measurements.

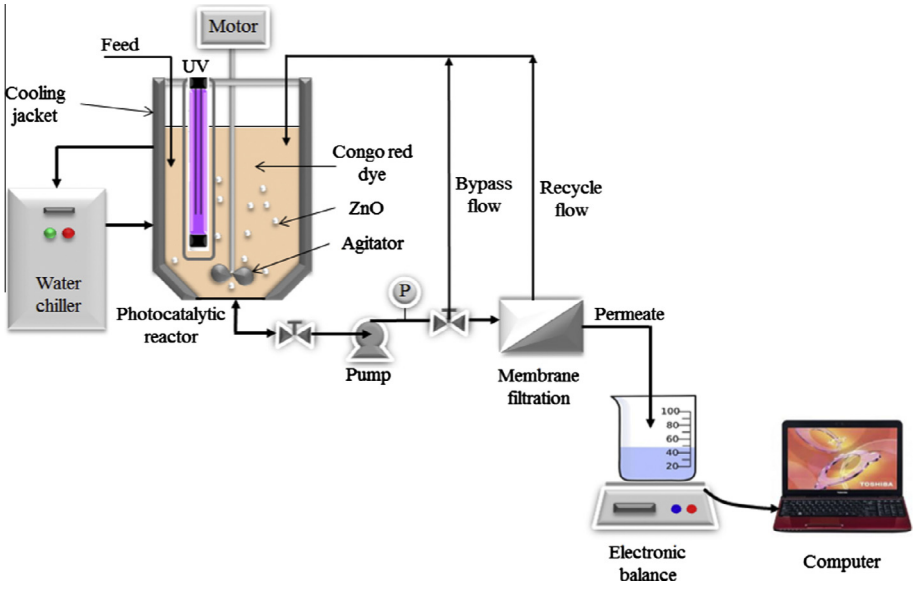

Fig. 1. Schematic diagram of the laboratory-scale MPR.

was used without any further purification. Reverse osmosis (RO) water was throughout employed as solvent. A working solution of 20 mg L^{-1} was prepared for the dye. The pH adjustments of the solution were made by adding a small amount of hydrochloric acid (HCl) or Sodium hydroxide (NaOH) solutions, received from R&M Chemicals, U.K. The pH of solution was measured with a microprocessor pH metre (Sastec ST-PHS3BW Model).

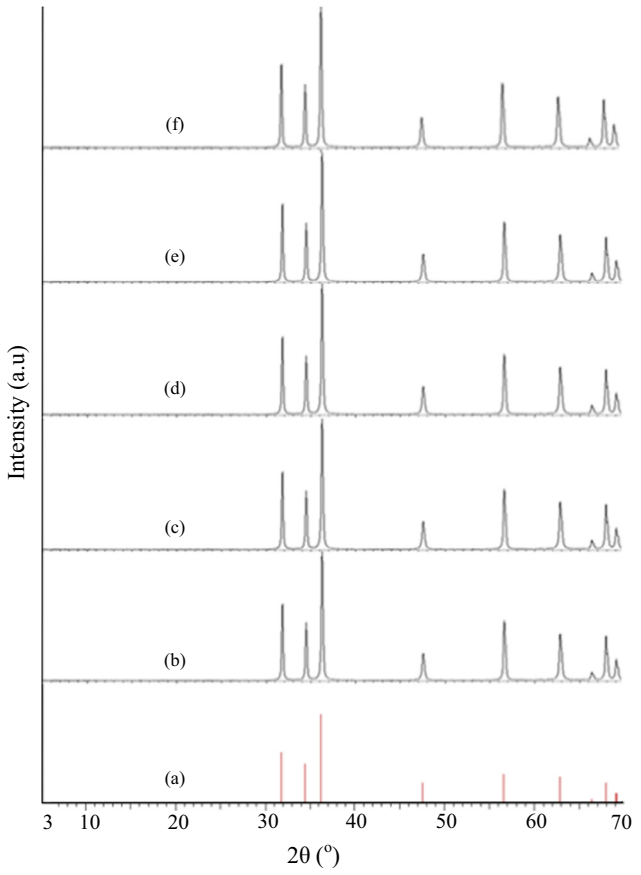

Fig. 2. XRD patterns of (a) standard ZnO peaks, (b) commercial ZnO, (c) ZnO-St (d) ZnO-Us, (e) ZnO-PVP-St and (f) ZnO-PVP-Us.

2.4. Experimental setup and operation

Schematic diagram of the laboratory-scale MPR is shown in Fig. 1. Before starting the dye purification, the membrane sample was wetted by circulating RO water in the MPR under 6 bar for 30 min to avoid compaction of the membrane. The effective membrane area was 22.90 cm^2. Five litres of photocatalytic reactor was used for operation either in batch or continuous methods. A UV lamp (253.7 nm, 18 W, GPH295T5L 4PSE, USA) was placed inside the reactor for activation of the photocatalyst. 0.1–0.5 g L^{-1} of photocatalyst (ZnO) was added into 20 mg L^{-1} of CR solution (pH 7) in the reactor. Before starting the photocatalysis process, the mixture was well agitated at 300 rpm for 30 min in the dark to reach adsorption–desorption equilibrium of the photocatalyst. The PL111 model of impeller with WiseStir® HS-50A overhead stirrer was used. The operation temperature was kept constant at 25 °C by recirculating cooling water with a water chiller (SP H2O model). After a 4 h photocatalysis process, the degraded dye was sampled and then flowed into the stainless steel flat sheet membrane module, 9.8 cm × 9.8 cm × 5.1 cm using a masterflex peristaltic pump at trans-membrane pressure of 6 bar. The degraded dye and ZnO after the photocatalysis process was separated using centrifuge (Eppendorf, 5804 model), for 20 min. The permeate was collected in a reservoir tank and weighed by an electronic balance (AND GF-6100, Japan). Subsequently, the weighing data were automatically transferred to a computer through the programme installed (RsKey Ver. 1.34).

2.5. Analytical method

The colour intensity of CR was measured using a UV–Vis spectrophotometer (ThermoSpectronic, Genesys 10uv) at the maximum absorption wavelength, λ_{max} = 510 nm. The colour removal was calculated through Eq. (1):

Table 2
Analysis of XRD.

Sample	Crystallite size (nm)
Commercial ZnO	51
ZnO-St	62
ZnO-Us	54
ZnO-PVP-St	7
ZnO-PVP-Us	12

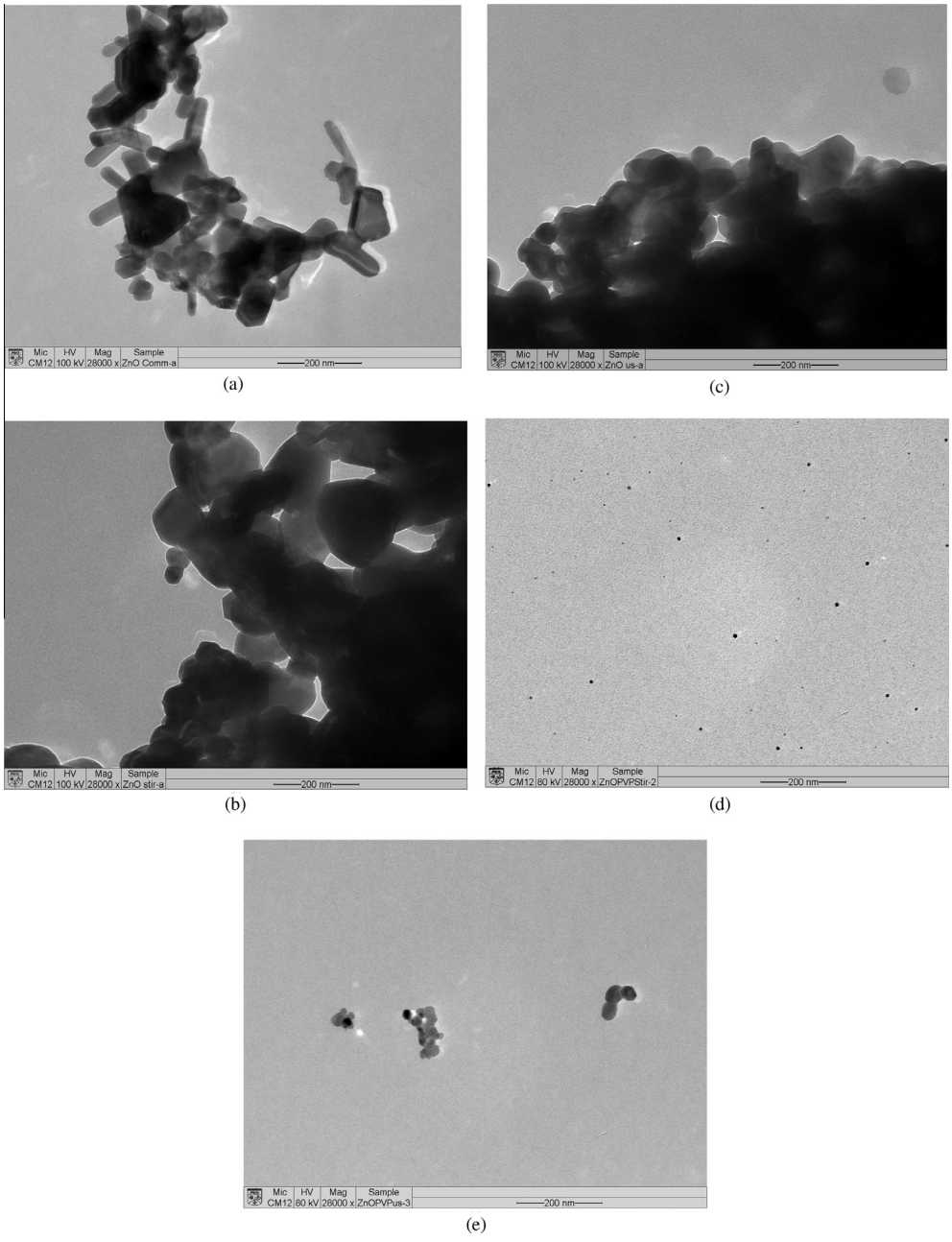

Fig. 3. TEM image of (a) commercial ZnO, (b) ZnO-St, (c) ZnO-Us, (d) ZnO-PVP-St and (e) ZnO-PVP-Us.

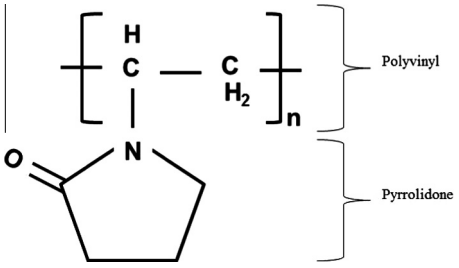

Fig. 4. Pyrrolidone and polyvinyl part of PVP.

$$\text{Colour removal} = \left(1 - \frac{C_f}{C_o}\right) \times 100\% \quad (1)$$

where C_f = final concentration and C_o = initial concentration.

Normalised flux of the membranes was calculated in order to study the behaviour of membrane fouling, since the membranes used in this study had different molecular weight cut-offs (Eq. (2)). A comparison study of the fouling behaviours was performed by plotting the graph normalised flux vs. operation time.

$$\text{Normalised flux} = \frac{\text{Solution flux, } J}{\text{Pure water flux, } J_o} \quad (2)$$

The percentage of relative flux reduction (RFR) or membrane fouling was calculated as follows:

$$\text{RFR} = \left(1 - \frac{J}{J_o}\right) \times 100\% \quad (3)$$

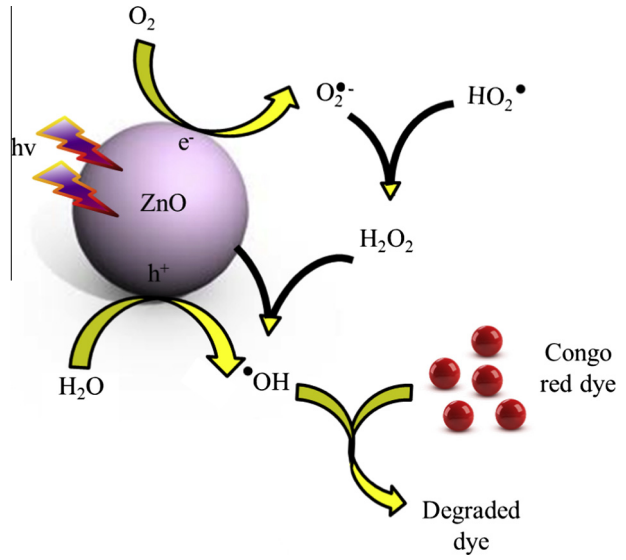

Fig. 5. Proposed photocatalytic degradation mechanism of CR dye using ZnO photocatalyst.

Table 3
Percentage of CR removal after photodegradation and nanofiltration in MPR with the absence/presence of photocatalyst.

Types of ZnO	CR degraded after photocatalysis (%)	CR removal after nanofiltration (%)
ZnO-PVP-St	72 ± 1.0	100 ± 0.5
ZnO-PVP-Us	65 ± 1.0	100 ± 0.5
ZnO-Us	56 ± 1.0	100 ± 0.5
ZnO-St	53 ± 1.0	100 ± 0.5
Commercial ZnO	45 ± 1.0	100 ± 0.5
No ZnO	0	100 ± 0.5

3. Results and discussion

3.1. Characterisation of ZnO nanoparticles

Fig. 2 shows the XRD patterns of commercial ZnO, ZnO-St, ZnO-Us, ZnO-PVP-St and ZnO-PVP-Us. The diffractograms of all the ZnO were quite similar to the standard ZnO peaks and commercial ZnO, which are well-matched with the typical single crystalline wurtzite hexagonal phase bulk ZnO [25]. No characteristic peaks of other impurities were detected in the pattern, indicating that the high purity of the ZnO via precipitation method under four different conditions had been successfully synthesised. The detailed analysis of the XRD is given in the Table 2. Crystallite size of the ZnO samples was calculated using Scherrer's formula:

$$CS = 0.9\lambda/\beta\cos\theta \quad (4)$$

where CS is the crystallite size, λ = 1.5406 Å, β is full width at half maximum (FWHM) of an *hkl* peak at θ value. The ascending order of the crystallite size is ZnO-PVP-St < ZnO-PVP-Us < commercial ZnO < ZnO-Us < ZnO-St. It can be deduced that without the PVP addition, precipitation under ultrasonic radiation generate the smaller ZnO as well as the commercial ZnO, compared to the reaction under vigorous stirring. This may be due to the slow reaction under ultrasonic radiation ultimately results in small crystal growth in the water. However, the presence of PVP in the precipitation reaction yielding much smaller crystallite size of ZnO nanoparticles. The smallest crystallite size of ZnO-PVP-St may be due to the fast and long-time reaction with the PVP which eventually results in small and uniform crystal growth in the water.

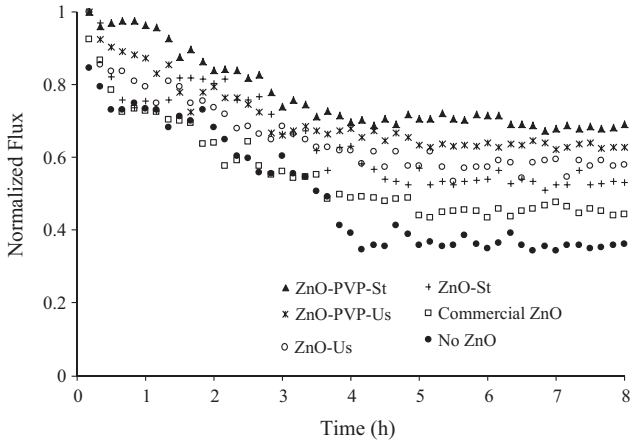

Fig. 6. Flux decline during the constant pressure nanofiltration of 20 mg L^{-1} and pH 7 of CR solutions at 6 bar, in the absence/presence of various ZnO.

The morphology and particle size of all ZnO were observed with TEM as shown in Fig. 3. It can be observed that the commercial ZnO consists of non-uniform shapes and agglomerated with large particle size in the range 50–140 nm. Agglomeration particles were also observed for ZnO-Us and ZnO-St in Fig. 3(b) and (c); however, they had a uniform size with large particle size of 50–130 nm and 40–150 nm, respectively. Interestingly, the precipitation of ZnO in the presence of PVP resulted in reducing agglomeration under ultrasonic radiation (Fig. 3(d)) with a smaller particle size in the range 12–42 nm. In fact, no agglomeration was observed for ZnO synthesised in the presence of PVP under stirring conditions (ZnO-PVP-St) with the smallest particle size, 7–30 nm as shown in Fig. 3(e). This is according to the pyrrolidone part (hydrophilic) and the polyvinyl part (hydrophobic) of PVP, as illustrated in Fig. 4. The PVP may control the growth of ZnO nanoparticles by forming passivation layers around the ZnO centre through coordination bond creation between the nitrogen atom of the PVP and the Zn^{2+} ion. Besides, due to the steric effect among the polyvinyl groups, the PVP possibly prevents ZnO agglomeration. However, the addition of a large quantity of PVP on the nanoparticles may cause destabilisation due to the osmotic pressure between their polymeric chains [26]. From the results, the ascending order of average particle size for all ZnO samples is ZnO-PVP-St < ZnO-PVP-Us < commercial ZnO < ZnO-Us < ZnO-St, which is well-matched with the crystallite size result. It could be deduced that the presence of PVP under stirring conditions not only prevents the agglomeration of nanoparticles, but also produced much smaller nanoparticles. In addition, it is expected that ZnO-PVP-St could provide better performances in MPR due to its morphology and smallest particle size.

3.2. Effect of the presence/absence and various types of the ZnO

The experiments were carried out in the absence of ZnO and presence of all ZnO samples (0.3 g L^{-1}). The proposed photocatalytic degradation mechanism was summarised in Fig. 5 according to the previous reports [6,27]. Table 3 presents the results obtained after photodegradation and nanofiltration processes for various parameters. The data shows a clear trend of decreasing photodegradation efficiency in the order of ZnO-PVP-St (72 ± 1.0%) > ZnO-PVP-Us (65 ± 1.0%) > ZnO-Us (56 ± 1.0%) > ZnO-St (53 ± 1.0%) > Commercial ZnO (45 ± 1.0%) > No ZnO (0). Generally, the particle size of the photocatalysts is reasonable for this result due to their effective

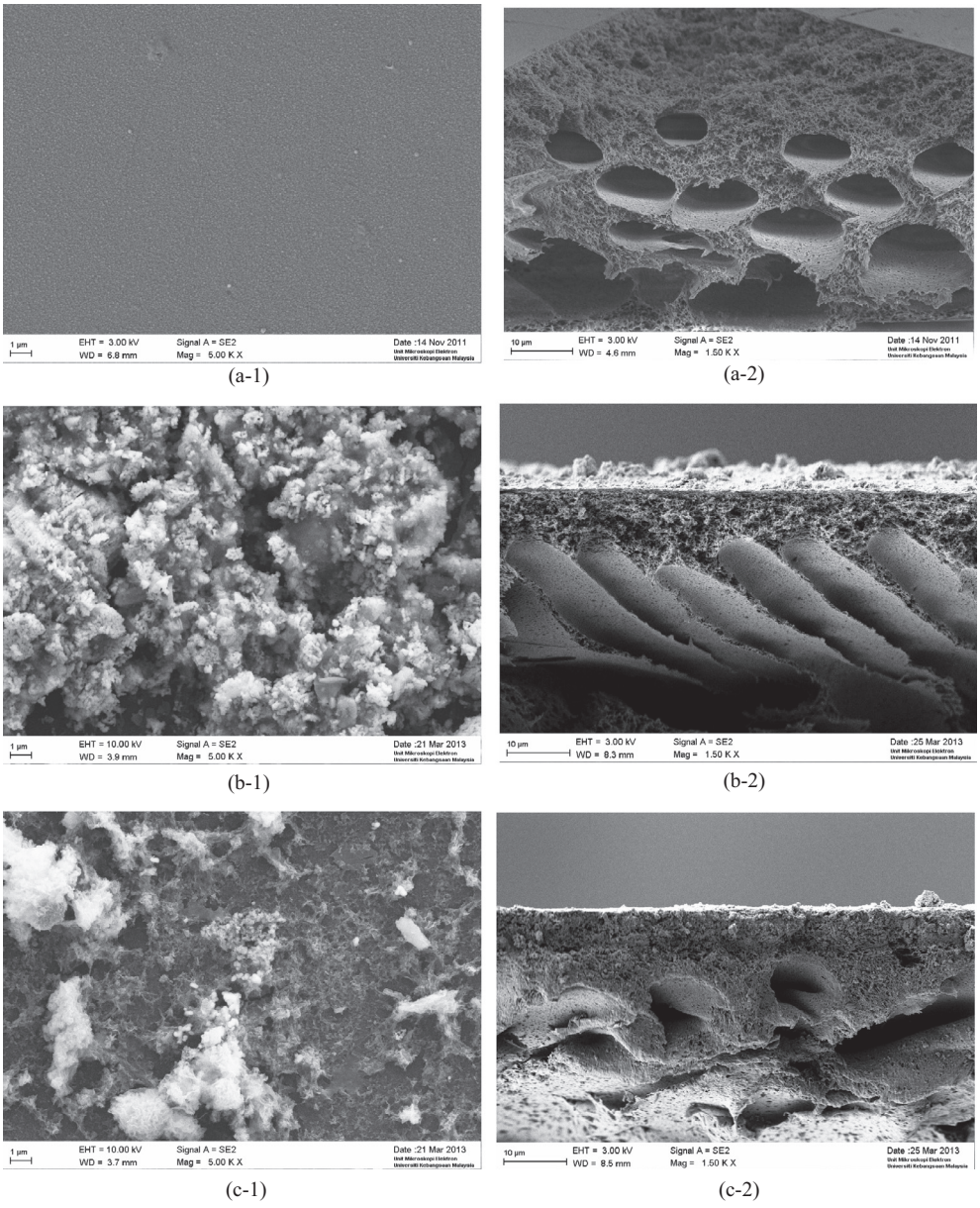

Fig. 7. Surface and cross-sectional area FESEM image of (a-1, 2) the NF membrane before filtration, (b-1, 2) the NF Membrane after filtration (in the absence of ZnO) and (c-1, 2) the NF Membrane after filtration (in the presence of ZnO-PVP-St).

surface area. However, there was a significant difference between the results compared to the order of average particle size, as specified in the Section 3.1. Therefore, the finding of the current study might be associated with the agglomerations (Fig. 3) and preparation route of the ZnO [9]. It can be deduced that the lesser the agglomerations, the better the photocatalytic activity of ZnO. This is mainly due to the effective surface area of the photocatalyst being able to adsorb the UV light, which causes the formation of an electron–hole pair on the photocatalyst surface (Fig. 5).

In the absence of photocatalysts, it was clearly seen that no dye degradation occurs under this condition. The result confirms that the presence of photocatalyst is very important in MPR to obtain the efficient pre-treatment system. Among the presence of all different types of ZnO in the photocatalysis, commercially available ZnO showed the worst performance, possibly due to the severe agglomerations and its inappropriate preparation method. This finding is in agreement with the recent study [6] which reported that the lower photodegradation efficiency of the commercially available ZnO in MPR was caused by the structural defects due to its preparation method. As expected, ZnO-PVP-St showed the most effective performances in the pre-treatment system. Thus, it can be deduced that the precipitation of ZnO was found to be a valuable method in producing the efficient nanoparticles, especially under stirring conditions in the presence of PVP.

Fig. 6 demonstrated the behaviour of flux decline for nanofiltration after photocatalysis process in the MPR with the ascending order of final normalised flux is in the presence of ZnO-PVP-St (33 ± 1.0%) < ZnO-PVP-Us (37 ± 1.0%) < ZnO-Us (42 ± 1.0%) < ZnO-St (47 ± 1.0%) < Commercial ZnO (56 ± 1.0%) < No ZnO (64 ± 1.0%). It was found that there was a significant positive correlation between the flux decline and the ZnO effectiveness, since the photocatalysis was represented as the pre-treatment process in MPR. CR removal of 100 ± 0.5% was achieved after all of the nanofiltration processes (Table 3). The results confirmed that all of the not degraded CR dye was successfully retained, which is the primary cause of the different membrane fouling behaviour. This is

Table 4
EDX analysis of the NF membrane.

Condition/ element	Fresh NF (Atomic %)	Fouled NF without ZnO (Atomic %)	Fouled NF in the presence of ZnO-PVP-St (Atomic %)
Carbon (C)	78.52	78.43	59.21
Oxygen (O)	18.27	17.91	29.64
Sulphur (S)	3.03	3.35	1.45
Sodium (Na)	0.18	–	–
Iron (Fe)	–	0.31	0.90
Chromium (Cr)	–	–	0.28
Aluminium (Al)	–	–	0.20
Silicon (Si)	–	–	0.29
Zinc (Zn)	–	–	8.03
Totals	100.00	100.00	100.00

due to the amount of dye deposited/adsorbed per unit of membrane surface area, which might be proportional to the percentage of flux decline [28]. Therefore, the maximum membrane flux decline (64 ± 1.0%) during the nanofiltration in the absence of photocatalyst is primarily due to the deposited of 100% of 20 mg L^{-1} dyes on the membrane surface. In addition, it is believed that the small amount of ZnO deposited, osmotic pressure enhancement and electrical double layer reduction could also be the cause of the flux decline behaviour [29]. It could be concluded that the presence of ZnO-PVP-St as the photocatalyst improves the NF membrane fouling and effectiveness of the MPR.

3.3. FESEM and EDX analysis

Fig. 7 and Table 4 show the FESEM image (surface and cross section) and EDX results of the NF membrane; before and after filtration process. It was clearly observed that many contaminants were trapped on the membrane surface after the nanofiltration process in the absence of ZnO photocatalyst, in comparison to the presence of ZnO-PVP-St. This was due to the deposition of larger amounts of non-degraded CR (Table 3) on the membrane surface, leading to the formation of a cake layer which is the primary cause of the membrane fouling (Fig. 6). The cross-sectional pattern was obviously changed after the filtration, mainly due to the pressure supply. Furthermore, penetration of the dye particle and impurities into the membrane pores may also be the cause of significant changes in the absence of ZnO condition.

From the EDX analysis, the elements existing after nanofiltration without photocatalyst were definitely due to the chemicals and impurities from CR. The atomic percentage of carbon (C) and sulphur (S) were decreased after nanofiltration in the presence of ZnO-PVP-St, possibly due to the smaller amount of CR from the photodegradation process. The increasing percentage of zinc (Zn) and oxygen (O) clearly demonstrated that the small amount of ZnO-PVP-St was retained from passing through the membrane pores. Moreover, it is also believed that the remaining ZnO was reused as the photocatalyst. The presence of the other elements may be due to the chemicals and impurities from the CR, ZnO-PVP-St and NF membrane surface.

Table 5
Percentage of CR removal after photodegradation and nanofiltration in MPR with various photocatalyst loading.

ZnO-PVP-St loading (g L^{-1})	CR degraded after photocatalysis (%)	CR removal after nanofiltration (%)
0.1	23 ± 1.0	100 ± 0.5
0.3	65 ± 1.0	100 ± 0.5
0.5	44 ± 1.0	100 ± 0.5

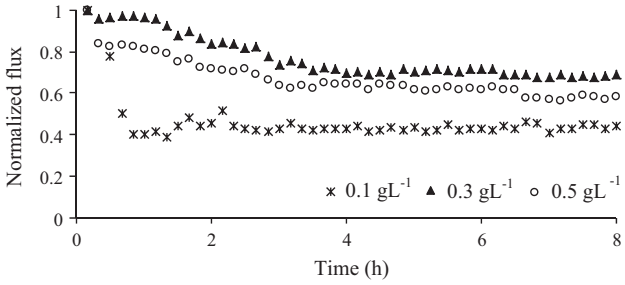

Fig. 8. Flux decline during the constant pressure nanofiltration of 20 mg L^{-1} and pH 7 of CR solutions at 6 bar, in the presence of ZnO-PVP-St with various photocatalyst loading.

3.4. Effect of ZnO-PVP-St loading

In order to obtain the optimum photocatalyst loading, the photodegradation of CR with varying ZnO-PVP-St loading from 0.1 to 0.5 g L^{-1} through the constant initial dye concentration (20 mg L^{-1}) at pH 7 was conducted. The degradation result (Table 5) and membrane flux decline behaviour (Fig. 8) obviously revealed that 0.3 g L^{-1} was the optimum ZnO loading. This is due to the effective surface of ZnO-PVP-St and adsorption of UV light, since there was an optimum amount of photocatalyst loading under different experimental conditions [30,31]. It is believed that 0.3 g L^{-1} of ZnO-PVP-St presented the maximum efficiency on photodegradation of CR (65 ± 1.0%) which subsequently contributed the minimum effects on membrane fouling (~25%). However, 0.1 g L^{-1} of the photocatalyst was not be sufficient to absorb the maximum UV light which cause the worse photodegradation of dyes (23 ± 1.0%) and led to increase the membrane flux decline (~58%). For the increasing of photocatalyst loading (0.5 g L^{-1}), it can cause overlapping of the ZnO which leads to obstruction of the UV light adsorption. Therefore, this would also reduce the photodegradation efficiency and increase the membrane flux decline (Table 5).

4. Conclusion

Four different types of ZnO nanoparticles were successfully synthesised via the precipitation method using oxalic acid and zinc acetate solutions. The presence of PVP obviously reduced the agglomerations and average particle size of the ZnO, according to the ascending order ZnO-PVP-St < ZnO-PVP-Us < ZnO-Us < ZnO-St. From the photodegradation and membrane fouling results, the presence of ZnO-PVP-St photocatalyst significantly improved the effectiveness of the MPR in terms of minimum membrane fouling, which was also supported by the FESEM characterisations. EDX results confirm that the small amount of ZnO-PVP-St was retained from passing through the membrane pores, whilst the remaining ZnO was reused as the photocatalyst. Under the initial dye concentration of 20 mg L^{-1} at pH 7, it was found that the optimum photocatalyst loading is 0.3 g L^{-1} for the MPR system, due to the effective surface area of ZnO-PVP-St and adsorption of UV light. It can be concluded that the optimum dosage of ZnO-PVP-St nanoparticles has a great potential in MPR for industrial dye wastewater treatment with very minimum NF membrane fouling.

Acknowledgements

The authors wish to thank Universiti Kebangsaan Malaysia (UKM), Malaysia through a Grant Number dip-2012-01, the Ministry of Higher Education Malaysia (MOHE), Malaysia and Universiti Tun Hussein Onn Malaysia (UTHM), Malaysia for their financial and administrative support.

References

[1] S. Mozia, Photocatalytic membrane reactors (PMRs) in water and wastewater treatment. A review, Sep. Purif. Technol. 73 (2010) 71–91.
[2] S. Mozia, M. Tomaszewska, A.W. Morawski, A new photocatalytic membrane reactor (PMR) for removal of azo-dye acid red 18 from water, Appl. Catal. B Environ. 59 (2005) 131–137.
[3] S. Yang, J.-S. Gu, H.-Y. Yu, J. Zhou, S.-F. Li, X.-M. Wu, L. Wang, Polypropylene membrane surface modification by RAFT grafting polymerization and TiO_2 photocatalysts immobilization for phenol decomposition in a photocatalytic membrane reactor, Sep. Purif. Technol. 83 (2011) 157–165.
[4] R. Goei, Z. Dong, T.-T. Lim, High-permeability pluronic-based TiO_2 hybrid photocatalytic membrane with hierarchical porosity: fabrication, characterizations and performances, Chem. Eng. J. 228 (2013) 1030–1039.
[5] G.E. Romanos, C.P. Athanasekou, F.K. Katsaros, N.K. Kanellopoulos, D.D. Dionysiou, V. Likodimos, P. Falaras, Double-side active TiO_2-modified nanofiltration membranes in continuous flow photocatalytic reactors for effective water purification, J. Hazard. Mater. 211–212 (2012) 304–316.
[6] N.H.H. Hairom, A.W. Mohammad, L.Y. Ng, A.A.H. Kadhum, Utilization of self-synthesized ZnO nanoparticles in MPR for industrial dye wastewater treatment using NF and UF membrane, Desalin. Water Treat. (2014) 1–12.
[7] J.-H. Sun, S.-Y. Dong, Y.-K. Wang, S.-P. Sun, Preparation and photocatalytic property of a novel dumbbell-shaped ZnO microcrystal photocatalyst, J. Hazard. Mater. 172 (2009) 1520–1526.
[8] R. Velmurugan, M. Swaminathan, An efficient nanostructured ZnO for dye sensitized degradation of reactive red 120 dye under solar light, Sol. Energy Mater. Sol. Cells 95 (2011) 942–950.
[9] K.G. Kanade, B.B. Kale, R.C. Aiyer, B.K. Das, Effect of solvents on the synthesis of nano-size zinc oxide and its properties, Mater. Res. Bull. 41 (2006) 590–600.
[10] M.A. Behnajady, N. Modirshahla, E. Ghazalian, Synthesis of ZnO nanoparticles at different conditions: a comparison of photocatalytic activity, Dig. J. Nanomater. Biostruct. 6 (2011) 467–474.
[11] K. Manzoor, S.R. Vadera, N. Kumar, T.R.N. Kutty, Energy transfer from organic surface adsorbate-polyvinyl pyrrolidone molecules to luminescent centers in ZnS nanocrystals, Solid State Commun. 129 (2004) 469–473.
[12] L. Saravanan, S. Diwakar, R. Mohankumar, A. Pandurangan, R. Jayavel, Synthesis, structural and optical properties of PVP encapsulated CdS nanoparticles, Nanomater. Nanotechnol. 1 (2011) 42–48.
[13] R. Hariharan, S. Senthilkumar, A. Suganthi, M. Rajarajan, Synthesis and characterization of daunorubicin modified ZnO/PVP nanorods and its photodynamic action, J. Photochem. Photobiol. A Chem. 252 (2013) 107–115.
[14] G. Shan, H. Hao, X. Wang, Z. Shang, Y. Chen, Y. Liu, The effect of PVP on the formation and optical properties ZnO/Ag nanocomposites, Colloids Surf. A Physicochem. Eng. Asp. 405 (2012) 1–5.
[15] S. Moradi, P.A. Azar, S.R. Farshid, S.A. Khorrami, M.H. Givianrad, Effect of additives on characterization and photocatalytic activity of Tio_2/ZnO nanocomposite prepared via sol–gel process, Int. J. Chem. Eng. 2012 (2012) 1–5.
[16] S. Lee, S. Jeong, D. Kim, S. Hwang, M. Jeon, J. Moon, ZnO nanoparticles with controlled shapes and sizes prepared using a simple polyol synthesis, Superlattices Microstruct. 43 (2008) 330–339.
[17] R.A. Damodar, S.-J. You, Performance of an integrated membrane photocatalytic reactor for the removal of reactive black 5, Sep. Purif. Technol. 71 (2010) 44–49.
[18] J.-T. Jung, J.-O. Kim, W.-Y. Choi, Performance of photocatalytic microfiltration with hollow fiber membrane, Mater. Sci. Forum. 544–545 (2007) 95–98.
[19] L. Djafer, A. Ayral, A. Ouagued, Robust synthesis and performance of a titania-based ultrafiltration membrane with photocatalytic properties, Sep. Purif. Technol. 75 (2010) 198–203.
[20] H. Jiang, G. Zhang, T. Huang, J. Chen, Q. Wang, Q. Meng, Photocatalytic membrane reactor for degradation of acid red B wastewater, Chem. Eng. J. 156 (2010) 571–577.
[21] R. Molinari, F. Pirillo, M. Falco, V. Loddo, L. Palmisano, Photocatalytic degradation of dyes by using a membrane reactor, Chem. Eng. Process. Process Intensif. 43 (2004) 1103–1114.
[22] R. Molinari, F. Pirillo, V. Loddo, L. Palmisano, Heterogeneous photocatalytic degradation of pharmaceuticals in water by using polycrystalline TiO_2 and a nanofiltration membrane reactor, Catal. Today 118 (2006) 205–213.
[23] S. Mozia, A.W. Morawski, M. Toyoda, M. Inagaki, Effectiveness of photodecomposition of an azo dye on a novel anatase-phase TiO_2 and two commercial photocatalysts in a photocatalytic membrane reactor (PMR), Sep. Purif. Technol. 63 (2008) 386–391.
[24] F.A. Pavan, S.L.P. Dias, E.C. Lima, E.V. Benvenutti, Removal of Congo red from aqueous solution by anilinepropylsilica xerogel, Dyes Pigm. 76 (2008) 64–69.
[25] R. Wahab, S.G. Ansari, Y.S. Kim, H.K. Seo, G.S. Kim, G. Khang, H.-S. Shin, Low temperature solution synthesis and characterization of ZnO nano-flowers, Mater. Res. Bull. 42 (2007) 1640–1648.
[26] R.G. Horn, Surface forces and their action in ceramic materials, J. Am. Ceram. Soc. 73 (1990) 1117–1135.
[27] N. Daneshvar, D. Salari, A.R. Khataee, Photocatalytic degradation of azo dye acid red 14 in water on ZnO as an alternative catalyst to TiO_2, J. Photochem. Photobiol. A Chem. 162 (2004) 317–322.
[28] M.M. Rao, D.K. Ramana, K. Seshaiah, M.C. Wang, S.W.C. Chien, Removal of some metal ions by activated carbon prepared from Phaseolus aureus hulls, J. Hazard. Mater. 166 (2009) 1006–1013.
[29] N. Hilal, H. Al-Zoubi, N.A. Darwish, A.W. Mohammad, M. Abu Arabi, A comprehensive review of nanofiltration membranes: treatment, pretreatment, modelling, and atomic force microscopy, Desalination 170 (2004) 281–308.
[30] H. Wang, C. Xie, W. Zhang, S. Cai, Z. Yang, Y. Gui, Comparison of dye degradation efficiency using ZnO powders with various size scales, J. Hazard. Mater. 141 (2007) 645–652.
[31] A. Akyol, H.C. Yatmaz, M. Bayramoglu, Photocatalytic decolorization of Remazol Red RR in aqueous ZnO suspensions, Appl. Catal. B Environ. 54 (2004) 19–24.